Polym. Bull. (2015) 72:931–961
DOI 10.1007/s00289-015-1308-5

REVIEW

Graphene modifications in polylactic acid nanocomposites: a review

H. Norazlina · Y. Kamal

Received: 21 July 2014 / Revised: 10 January 2015 / Accepted: 15 January 2015 /
Published online: 3 February 2015

Abstract Considerable interest has been devoted to graphene since this material has shown promising and excellent results in mechanical and thermal properties. This finding has attracted more researchers to discover the attributes of graphene due to its extensive and potential applications. This paper reviewed the recent advances in the modification of graphene and the fabrication of polylactic acid/graphene nanocomposite. The different techniques that have been employed to prepare graphene, such as reduction of graphene oxide and chemical vapor deposition, are discussed briefly. The preparations of PLA/graphene nanocomposites are described using in situ polymerization, solution, and melt blending; and the properties of these nanocomposites are reviewed. Due to the difficulties in obtaining good dispersions, modifications of nanomaterials have been the critical issues that lead to excellent mechanical properties.

Keywords Polylactic acid · Graphene · Graphene modifications · PLA/graphene nanocomposites

Introduction

The attributes of graphene, namely transparency, density, electric and thermal conductivities, elasticity, flexibility, hardness, and mechanical resistance, as well as the capacity to generate chemical reactions with other material, have been a

H. Norazlina (✉)
Faculty of Chemical Engineering Technology, TATI University College,
24000 Kemaman, Terengganu, Malaysia
e-mail: norazlinatatiuc@gmail.com

Y. Kamal
Faculty of Chemical and Natural Resources Engineering, University of Malaysia Pahang,
26300 Gambang, Pahang, Malaysia

potential port to release a revolutionary new technology. In 2004, a group of researchers studied the preparation and the isolation of single graphene layers using adhesive tape. They measured the electric properties of the flakes [1], and thus, boosted the current research.

There are many different types of graphene-based materials, and they can be categorized by limiting them into groups of graphene, graphene oxide, graphite, expanded graphite, and graphite oxide. The properties are different, depending on where the graphene sits within this space. Each graphene type is manufactured using different techniques, and all techniques differ in terms of their cost structure, volume production capability, and ultimately, potential target markets. The manufacturing techniques include micro-cleavage, chemical vapor deposition, liquid-phase exfoliation, oxidization–reduction, and plasma.

Polylactic acid (PLA) is considered both; (1) biodegradable, which is suitable for short-term packaging, and (2) biocompatible in contact with living tissues, as it is appropriate for medical applications, such as tissue scaffolds, internal sutures, and implant devices [2]. Since the basic monomers (lactic acid) are produced from renewable resources (carbohydrates) via fermentation, this compostable material reduces the solid waste disposal problem. Amazingly, due to the depletion of petroleum resources, PLA has entered into a new era as a valuable biosource polymer alternative in long-term applications, such as automotive and electronics. Unfortunately, some disadvantages, such as relatively poor mechanical properties, slow crystallization rate, and low thermal resistance, have limited its application. As an alternative, adding nanofillers has been an interesting way to improve the properties and to expand the use of PLA.

Polylactic acid (PLA)

Polylactic acid or polylactide (PLA) belongs to the family of aliphatic polyesters, commonly made from α-hydroxy acids. PLA is a polymer, in which, the stereochemical structures can be modified by polymerization of the controlled mixture of L and D isomers to yield high molecular weight and amorphous or semi-crystalline polymers. In addition, the properties of PLA can be easily modified through the addition of plasticizers, fillers, other biopolymers, etc. In 2010, a market survey showed that the PLA was in the second place at demand after starch-based plastic in biobased plastic category for global demand [3].

Besides, there are several ways to synthesize PLA, which involve two monomers: lactic acid and cyclic di-ester, lactide. The most common method is the ring-opening polymerization of lactide with various metal catalysts (mostly tin octoate) in solution, melt or as a suspension, patented by Cargill (US) in 1992 [4]. The second route to PLA is the direct condensation of lactic acid monomers below 200 °C. This method consists of two stages: (1) lactic acid first oligomerized to PLA oligomers; (2) polycondensation is done in the melt or as solution, whereby short oligomeric units are combined to give high molecular weight polymer. This route needs water removal through the application of vacuum or azeotropic distillation to favor polycondensation over transesterification [5]. PLA has varying molecular

weights, and only high molecular weight is used in the packaging industry (Fig. 1; Table 1).

Properties of PLA

Lactic acid is a chiral molecule that exists in L and D isomers, and the term "polylactic acid" refers to a family of polymers, which are pure poly-L-lactic acid (PLLA), pure poly-D-lactic acid (PDLA), and poly-D,L-lactic acid (PDLLA) [12]. The final properties of PLA depend more on the content in optical impurities between both LA enantiomers within PLA chains. PLA can be tailored by a formulation involving co-polymerizing of the lactide with other lactone-type monomers, and hydrophilic macromonomers, such as polyethylene glycol (PEG) or other monomers, with functional groups, such as amino and carboxylic groups, and blending PLA with other materials [13] (Table 2).

PLA is thermally unstable and exhibits rapid loss of molecular weight, which is a result of random main-chain scissions. PLA degradation occurs in two stages: (1) random non-enzymatic chain scission of the ester groups that leads to a reduction in molecular weight, and (2) the molecular weight is reduced until the lactic acid and low molecular weight oligomers are naturally metabolized by microorganisms to produce carbon dioxide and water [16, 17]. Several reactions, such as hydrolysis, de-polymerization, inter-, and intra-molecular transesterification reactions to monomer and oligomeric esters, are involved in the degradation process during thermal reactions [15, 18]. The thermal degradation is initiated below the PLA melting point and the rate rapidly increases above the melting point.

In addition to its biodegradability, PLA exhibits a Young modulus of around 3 GPa and impact strength close to 2.5 kJ/m^2 [19]. By comparison with commodity polymers, such as polyethylene (PE), polypropylene (PP), polystyrene (PS), and polyethylene terephthalate (PET) [20], the mechanical properties of semi-crystalline PLLA are attractive, especially Young modulus, as PLA is favored for short-term

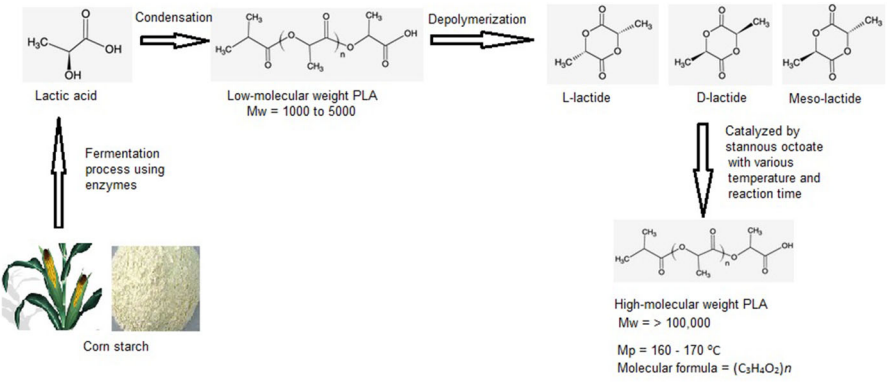

Fig. 1 PLA production steps by ring-opening polymerization using stannous octoate as an initiator

Table 1 A summary of studies on PLA polymerization variables and molecular weight, catalyzed by stannous octoate

Lactic acid polymers	Solvent(s)	Reaction temp. (°C)	Reaction time	Molecular weight	References
PDLLA, PLLA	Alcohols	200	60–75 min	$M_w < 350{,}000$	Korhonen et al. [6]
PLLA	Glycerol	130	6 h	$DP_n = 43–178$	Han et al. [7]
PLLA, PDLA	Alcohols, carboxylic acid	130	2–72 h	$M_n < 250{,}000$	Zhang et al. [8]
PLLA	No solvent	130	72 h	$M_v = 20{,}000–680{,}00$	Hyon et al. [9]
PLLA (stannous octoate and triphenylamine)	No solvent	180–185	7 min	$M_n = 91{,}000$	Jacobsen et al. [10]
PLLA (stannous octoate and compounds of titanium and zirconium)	Toluene	180–235	15–180 min	$M_n = 40{,}000–100{,}000$	Rafier et al. [11]

Table 2 Lactic acid polymer properties (represents the values from [14, 15])

Lactic acid polymers	Glass transition temperature T_g (°C)	Melting temperature T_m (°C)	Density (g/cm^3)	Good solubility in solvents
PLLA	55–80	173–178	1.290	Chloroform, furan, dioxane, and dioxolane
PDLLA	43–58	120–170	1.25	PLLA solvents and acetone
PDLA	40–50	120–150	1.248	Ethyl lactate, tetrahydrofuran, ethyl acetate, dimethylsulfoxide, *N*,*N* xylene, and dimethylformamide

packaging. Unfortunately, PLA is a brittle material with low impact strength, resulting in limitation for the sustainable development of PLA [16] and the low crystallization ability limits the industrial implementation [21] (Table 3).

The physical, mechanical, and barrier properties of PLA depend on the solid-state morphology and its crystallinity. PLA can be either amorphous or semi-crystalline, depending on its stereochemistry and thermal history. The favorable of crystallinity formation relies on the end-use requirement of PLA. For instance, high crystallinity is unnecessary for injection molded, which is pursued for further blow molding since rapid crystallization of the PLA would hamper the stretching of the performance and the optical clarity of the resulting bottle [23]. Otherwise, increased crystallinity is desirable for injection-molded articles, for which good thermal stability is important. Two strategies can be implemented to increase crystallinity [23]: (1) annealing the PLA between the glass transition temperature and the melting temperature to improve the thermal stability, and (2) incorporating nanoparticles as nucleating agent in the PLA during extrusion. These lower the

Table 3 Comparison between the properties of PLA and other polymers (represents the value from [22])

	T_g (°C)	T_m (°C)	Tensile strength (MPa)	Tensile modulus (MPa)	Elongation at break (%)
PLA	40–70	130–180	48–53	3,500	30–240
LDPE	−100	98–115	8–20	300–500	100–1,000
PCL	−60	59–64	4–28	390–470	700–1,000
PS	70–115	100	34–50	2,300–3,300	1.2–2.5
PVA	58–85	180–230	28–46	380–530	–
PET	73–80	245–265	48–72	200–4,100	30–300

LDPE low density polyethylene, *PCL* polycaprolactam, *PS* polystyrene, *PVA* polyvinyl alcohol, *PET* polyethylene terephthalate

surface free energy barrier for nucleation and allow crystallization at higher temperature to take place upon cooling.

Recently, melt processing has been the main conversion for the approaches of PLA. Hence, comprehension on thermal, crystallization, and melt rheological behavior is vital to optimize the properties of PLA. The rheological properties are highly dependent on temperature, molecular weight, and shear rate. Semi-crystalline PLA tends to possess higher shear viscosity than its amorphous counterpart under identical processing conditions. As shear rate increases, the viscosities of the melt decrease significantly [24]. The rheological properties of PLA can be tailored by the insertion of branching into the polymer chain architecture using variety routes like multifunctional polymerization initiators, hydroxycyclic ester initiators, multicyclic ester, and crosslinking via free radical addition [25–28].

Graphene-based materials

Graphite, as a carbon natural precursor, is made of hundreds of thousands of layers of graphene. Graphite is naturally a very brittle compound and cannot be used as a structural material on its own due to its sheer planes. Extensive research has proven that graphite is an impressive mineral that shows a number of outstanding and superlative properties, including its ability to conduct electricity and heat well, also highly resistant to chemical attack and self-lubricating. Graphite is one of the only three naturally occurring allotropes of carbon, besides diamond and amorphous carbon. The differences between the three naturally occurring allotropes are the structure and the bonding of the atoms within the allotropes; diamond enjoying a diamond lattice crystalline structure, graphite having a honeycomb lattice structure, and amorphous carbon is without a crystalline structure.

Graphene is a thin layer of pure carbon, which is a single, and a tightly packed layer of carbon atoms that are bonded together in a hexagonal honeycomb lattice. It is an allotrope of carbon in the structure of a plane of sp^2-bonded atoms. Graphene is the basic structural element of other allotropes, such as graphite, charcoal, carbon nanotube, and fullerenes. Graphene sheets stack to form graphite with an interplanar

spacing of 0.335 nm and the carbon–carbon length in graphene is about 0.142 nm [29].

The awareness of graphene began to take place in 1859 when Brodie realized the highly lamellar structure of thermally reduced graphite oxide [30]. Thereafter, many scientists have been involved in graphene researches [31–40]. The revolution of graphene has sparked in 2004 [1], whereby they extracted single-atom-thick crystallites from bulk graphite using Scotch tape or mechanical cleavage technique. For this effort, they were awarded Nobel Prizes in Physics in 2010. In 2009, graphene became one of the strongest materials, known with a breaking strength over 100 times greater than hypothetical steel with similar thickness [41] and stiffness of 1,000 GPa [42] and 220 Gpa for graphene oxide (GO) [43]. The fracture strength of a single-layer graphene is 130 GPa [42] with thermal conductivity ~5,000 W/mK [44] and electrical conductivity 10^4 S/cm [45]. The value of thermal conductivity is significantly higher than GO (~2,000 W/mK) [42], multiwall carbon nanotubes (~3,000 W/mK) and single-wall carbon nanotubes (~3,500 W/mK) [46, 47]. Besides, graphene also shows excellent electric charge transport and 97.7 % optical transmittance [48]. High light transmittance, photoluminescence, and high charge mobility are features of graphene that are important for applications in Magnetic Resonance Imaging (MRI) and biomedical imaging [49, 50].

Pristine graphene is hydrophobic in nature and it poorly disperses in water, which requires surfactants or other stabilizing agents to obtain suspension in biological fluids and to prevent agglomeration [51]. Graphene oxide is capable in forming hydrogen bonds and metal ion complexes due to the polar basal plane and negative charges associated with carboxylate groups on the edge site [52]. Reduced graphene oxide consists of basal vacancy defects that occur during oxygen removal, making it less hydrophobic than graphene and shows less basal reactivity than graphene oxide [52–55].

Graphene has great potential for applications in medicine, electric circuits, chemical and industrial processes. In 2008, graphene produced from exfoliation procedures had been scaled up and manufacturers sold graphene in large quantities [56]. In early 2013, the European Union awarded a grant worth of one billion Euros to be used for research of potential graphene applications [57]. With the rapid development of synthesis and functionalization approaches, graphene and its related derivatives have shown prominent potentials in many fields such as nanoelectronics [58, 59], composite materials [60–63], energy technology [64–67], sensors [68, 69], and catalysis [70–72].

Beyond the applications aforementioned, another interesting field, the biomedical application, is a relatively new area for graphene-based nanomaterials due to their excellent mechanical, electrical, and optical properties. The 2D structure of graphene and the presence of delocalized surface π electrons can be used for effective drug loading via hydrophobic interactions and π–π stacking [51]. Several researches have been observed in this field using graphene oxide [73–76]. Another application of graphene in biomedical is as gene therapy to treat genetic disorders such as cancer, cystic disorders, and Parkinson's disease. The efficient and safe gene vectors that protect DNA from nucleus degradation, as well as in facilitating DNA

uptake with high transfection efficiency, are compulsory to obtain successful gene delivery [77, 78]. The approaches for the use of graphene in gene delivery are functionalized with cationic polymers such as polyethylenimine (PEI) [79–82], chitosan-functionalized GO [83], and amine-terminated PEGylated GO [84]. PEI is used as a non-viral gene vector due to its strong electrostatic interaction with negatively charged phosphates of RNA and DNA, and its chemicals are easily modified to achieve increased transfection efficiency, cell selectivity, and reduced cytotoxicity [51]. Furthermore, Chitosan–GO acts by thickening the pDNA into stable nano-sized complexes.

Routes of producing graphene

Chemical vapor deposition (CVD)

The most common way for scientists to create a monolayer or a few layers of graphene is by a method known as chemical vapor deposition (CVD), also known as "bottom-up". This is a method that extracts carbon atoms from a carbon-rich source by reduction. This method involves the growth of graphene films with macroscopic dimensions on the surface of metal. The main problem with this method is finding the most suitable substrate to grow graphene layers on, and also developing an effective way of removing the graphene layers from the substrate without damaging or modifying the atomic structure of the graphene. The first successful synthesis of a few layers of graphene films using CVD was reported in 2006 by Somani et al. [85], using camphor as the precursor on Ni foils. This research showed a new way of graphene synthesis route with several unsolved problems like controlling the number of layers and minimizing the folding of graphene.

Three processes can be classified in the CVD technique: (1) thermal CVD, (2) plasma-enhanced CVD, and (3) thermal decomposition on SiC and other substrates. In thermal CVD, two general approaches have been developed: (1) the precipitation of carbon from carbon-rich precursors on metal like nickel (Ni) [86] and cobalt (Co), and; (2) the CVD growth of carbon on copper (Cu) using methane (CH_4)/H_2 mixtures [87]. The diffusion of carbon into the metal thin film is involved during the growth of graphene on substrates with medium-high carbon solubility (>0.1 atomic %), such as Ni and Co, at the growth temperature, and the henceforth precipitation of carbon out of the bulk metal to metal surface upon the cooling [86, 88]. The thickness and crystalline ordering of the precipitated carbon (graphene layers) are controlled by the cooling rate and the concentration of carbon dissolved in the nickel, which is determined by the type and concentration of the carbonaceous gas in the CVD, and the thickness of the nickel layer [89].

On the other hand, as for route (2), the graphene growth on low carbon solubility (<0.001 atomic %) substrate like Cu priory happens on the surface through the four steps process described by Li et al. [87]: (1) first, catalytic decomposition of methane on Cu, (2) the formation of nuclei as a result of supersaturation, (3) nuclei grown to form graphene islands on Cu surface saturated or supersaturated, and finally, (4) full Cu surface coverage by graphene under certain temperature, methane flow rate, and methane partial pressure. A unique feature of CVD method in

synthesizing graphene is the possibility for substitutional doping by introducing other gases, such as NH_3, during growth [70, 90, 91]. A research found that the N-graphene electrode has long-term stability, tolerance to crossover, and better poison effect than Pt/C for oxygen reduction in alkaline electrolyte [70]. The reversible discharge capacitance of N-graphene in lithium batteries is almost double compared to pristine graphene because the surface defects are induced by nitrogen doping, as reported by Reddy et al. [91].

Then, the second technique of CVD, plasma-enhanced CVD (PECVD), offers the graphene synthesis at lower temperature and low pressure using reactive species generated in the plasma compared to thermal CVD. The benefits of the plasma deposition include very short deposition (<5 min) and lower growth temperature of 650 °C compared to thermal CVD (1,000 °C). The growth mechanism of graphene via PECVD is balanced between the graphene deposition through the surface diffusion of C-bearing growth species from precursor gas, and etching caused by atomic hydrogen [89].

In addition, Terasawa and Saiki [92] studied the graphene deposition on Cu using PECVD at 500 and 900 °C using CH_4/H_2 gas mixture. It has been pointed before; the dissociation hardly occurs at around 500 °C using thermal CVD, so, graphene does not grow at this temperature. In contrast, the activated carbon fragment like C_2 radical is formed in PECVD and the graphene growth occurs even at the temperature of 500 °C, as depicted in Fig. 2a, however, the grain size is limited to 20 nm. At higher temperature, as depicted in Fig. 2b, the catalytic nature of Cu works simultaneously and increases the grain size of the first graphene layer to 40 nm, as larger grain size of Cu substrate causes enlargement of graphene growing on it. As for the second layer of growth, the active sites are concentrated on C_2 and CH radicals. The attachment of C_2 radicals continues the growth of graphene, while the attachment of CH blocks the extension of sp^2 network. The effect of CH is

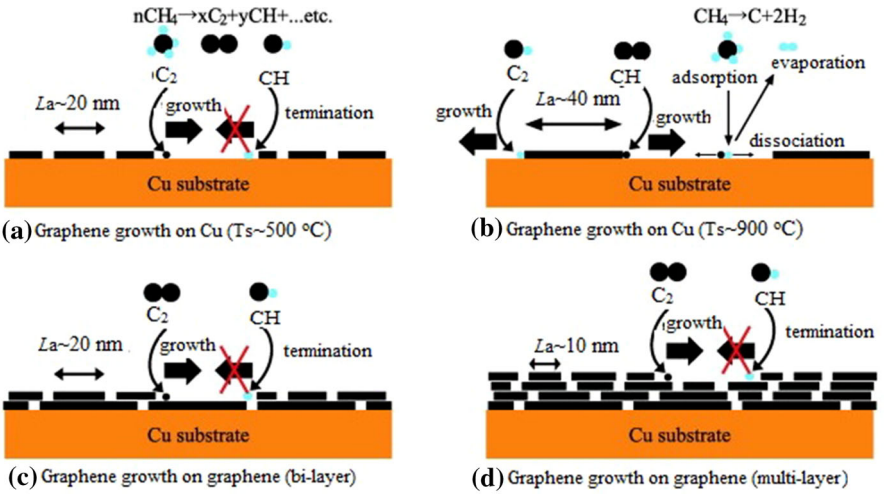

Fig. 2 The growth of graphene at 500 and 900 °C using PECVD method

presented in (a), (c), and (d). Hence, the size of graphene growth is limited by the degree of CH termination.

The third method of obtaining graphene is to heat silicon carbide (SiC) to high temperature (>1,100 °C) under low pressure (~10–6 torr) in a dense noble gas to reduce it to graphene [93]. The face of SiC used for graphene formation, either silicon or carbon-terminated, extremely influences thickness, mobility, and carrier density of the graphene. The important advances on graphene have been made since a patent for graphene-based electronics was filed provisionally in 2003 and was issued in 2006 [94]. This patent claims creating on a preselected face of a substrate, a thin-film graphitic layer disposed against preselected face; and generating a preselected pattern on the thin-film graphitic layer. In 2009, researchers at the Hughes Research Laboratories produced very high frequency transistors on monolayer graphene on SiC, where the epitaxial-graphene layer is formed by graphitization of 2-in-diameter Si-face semi-insulating 6H-SiC (0 0 0 1) substrates with a metal gate on top of a high-k Al_2O_3 gate dielectric deposited via an atomic-layer-deposition method [95], only after one year the researchers at MIT Lincoln Lab produced hundreds of transistors on a single chip [96]. The MIT Lincoln Lab developed transistors using multilayered epitaxial graphene (MEG) on SiC. In this research, graphitic films on SiC substrates were prepared by solid-state decomposition of single-crystal 4H-SiC (0 0 0 1) in vacuum. Si sublimes to produce carbon-rich surfaces that subsequently graphitize. When SiC substrate is heated under ultrahigh vacuum (UHV), the silicon atoms sublimate from the substrate and the removal of Si leaves the surface of the carbon atoms to be rearranged into graphene layers [89]. The thickness of graphene layers depends on the annealing and the temperature of UHV. Besides the interesting method of manufacturing graphene, several hurdles are encountered in the real production, such as controlling the thickness of graphene layers in large area production [89]. Another challenging issue is the different epitaxial growth patterns on different SiC polar face, Si-face, and C-face. Such mismatch of graphene growth process has visceral effects on the physical and electronic properties of epitaxial growth.

The epitaxial growth on metal substrates uses source and atomic structure of a metal substrate to start the growth of the graphene. Parga et al. [97], studied the (0 0 0 1) faces of ruthenium (Ru) crystals under UHV and found that the first graphene layer coupled strongly to the Ru substrate, while the second layer was free of the substrate interaction and had a similarity of electronic structure with free-standing graphene. In contrast, the graphene growth on Irridium (Ir) is uniform in thickness, weakly bonded, and can be produced in highly ordered [98]. Rafiee et al. [99] reported that graphene coatings did not significantly disrupt the intrinsic wetting behavior of surfaces for which surface–water interactions are dominated by van der Waals forces. Their findings indicated that the wetting transparency of graphene is related to its extreme thinness. According to Li et al. findings in 2009, the increasing of 30–40 % in condensation heat transfer on Cu using CVD method is as a result of the ability of the graphene coating to suppress Cu oxidation without disrupting the intrinsic wettability of the surface. The employment of Cu at low pressure using methane ends the growth of graphene automatically after the first single layer is

formed and large graphene films can be produced easily [87]. Besides, the use of ethane and propane gases leads to the growth of bi-layer graphene [100].

Among all the other techniques, graphene synthesized by CVD and epitaxial growth on metal substrate, especially copper, has large area [86–88, 101] and both single-layer and bi-layer characteristics with specific area up to 1 cm^2 for industrial and electronic applications, but unfortunately, this method fails to synthesize the bulk quantities of graphene [102].

Mechanical cleavage and liquid-phase exfoliation

The excellent properties of graphite, such as in-plane mechanical, structural, thermal, and electrical properties, are highly hinged on the exfoliation graphite down to single graphene sheets in the matrix. The main obstacle in the synthesis and the processing of bulk-quantity graphene sheets is aggregation. Graphene must be well separated from each other, otherwise, this material tends to form irreversible agglomerates or restack to form graphite through van der Waals interactions [89].

The simplest way of preparing small samples of single- or few-layer graphene is by the mechanical cleavage like the repeated peeling of graphene layers with adhesive tape [89]. Nevertheless, the large graphene surface area ($\sim$1 mm^2) obtained is an inadequacy in this method [1]. The consumption of graphite-intercalated compounds (GIC) could overcome this problem. Expanded graphite (EG) is produced from GIC by rapid evaporation of the intercalate component at high temperatures. Oxidants and other molecules could more easily enter in the interlayer space of EG compared to natural graphite because graphite could expand up to a hundred times in volume at high temperature due to thermal expansion of the evolved gas trapped between the graphene sheets [89].

Recently, Hassan et al. [103], produced high-yield aqueous phase exfoliation of graphene via in situ emulsion polymerization using EG. In the beginning of the research, thermal EG was produced, and followed by the preparation of dispersion in 20 mL distilled water by mixing 0.1 wt% EG with variable amounts of sodium dodecyl sulfate (SDS) as surfactant and stabilizing agent. Later, a sonication process for 60–80 min at room temperature took place and was continued by in situ emulsion polymerization to synthesize poly(styrene)–graphene nanocomposite. Non-exfoliated graphite is eventually separated from the graphene by centrifugation. The TEM results showed that the exfoliated graphene comprised of nanoflake with 60 % of $\leq$5 layers and 90 % of $\leq$10 layers of the product. Zhou et al. [104], synthesized high quality and high concentration of graphene sheets using EG via intercalation and exfoliation pathway using *n*-butyl lithium as intercalating agent, water, and *N*,*N*-dimethylformamide (DMF) as exfoliating agent.

Cutting open carbon nanotubes (CNT)

Graphene nanoribbons can be produced by the unzipping of multiwalled CNT (MWCNTs). In 2010, Terrones et al. [105], reviewed the methods to produce graphene nanoribbons by unzipping the CNT, as shown in Fig. 3. Figure 3a depicts an intercalation–exfoliation of MWCNTs, involving treatments in liquid NH_3 and

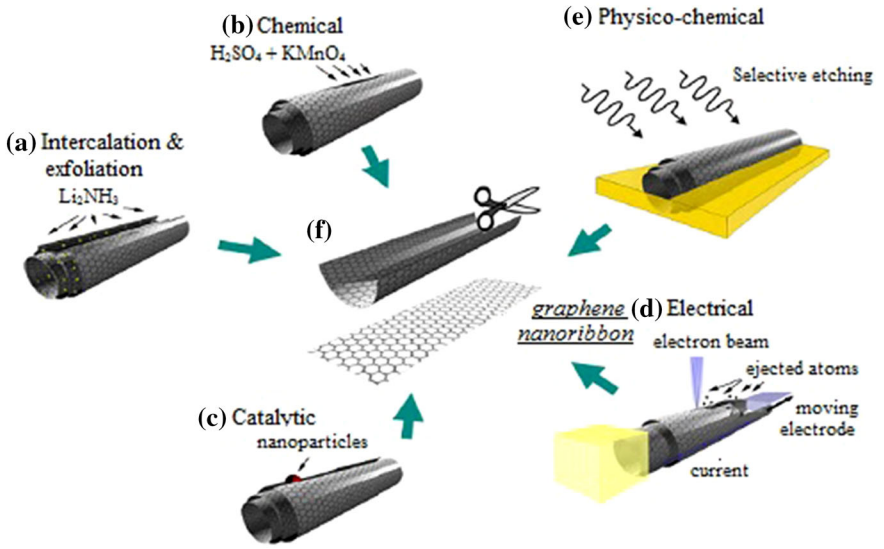

Fig. 3 The different ways nanotubes could be unzipped to yield graphene nanoribbons (GNRs)

Li, and followed by exfoliation using HCl and heat treatments; (b) chemical route by acid reactions that start to break carbon–carbon bonds, such as H_2SO_4 and $KMnO_4$ as oxidizing agents; (c) the implementation of catalytic approach as metal nanoparticles 'cut' the CNT longitudinally; (d) electrical method by passing an electric current through a CNT; and (e) physiochemical method by embedding the tubes in polymer matrix, followed by Ar plasma treatment. Figure 3f portrays the resulting structures, either GNRs or graphene sheets.

Carbon dioxide reduction

Chakrabarti et al. [106], from Northern Illinois University found a simple way to synthesize graphene. The synthesis process involves a highly exothermic reaction, in which, magnesium (Mg) is combusted in oxidation–reduction with carbon dioxide (either solid or gases), producing a variety of carbon nanoparticles, including graphene and fullerenes. The team showed that the graphene was formed in a few layers of nanosheets up to 10 atoms thick. Burning Mg metal in CO_2 environment produces carbon materials, as shown in the equation below:

$$2Mg(s) + CO_2(g) \rightarrow 2MgO(s) + C(s).$$

Recently, various approaches have been developed for the mass production of pure and high-quality graphene nanosheets (GNs) without oxidation and reduction process, including exfoliation of graphite using sonication [103], wet ball milling [107–109], and supercritical fluids (SCFs) processes [110, 111]. SCFs technique offers a low-cost and simple approach to a large-scale production of pure graphene

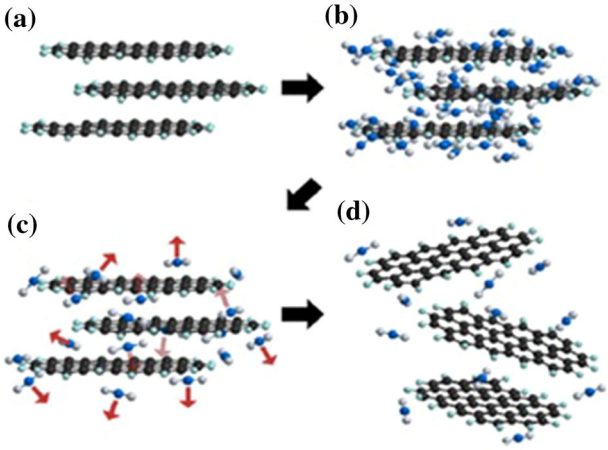

Fig. 4 Exfoliation mechanism of graphite through $scCO_2$ process

sheets without the need for complicated processing steps or chemical treatment. Pu et al. [105], implemented supercritical CO_2 processing technique for intercalating and exfoliating layered graphite. Few-layer graphene, which contains about 10 atomic layers, are produced by immersing powdered natural graphite in supercritical CO_2 for 30 min, followed by rapid depressurizing the SCFs to expand and to exfoliate graphite. Graphene are gathered by discharging the expanding CO_2 gas directly into a solution containing sodium dodecyl sulfate (SDS) to avoid restacking.

In 2012, Sim et al. [112], prepared the GNs through repeated supercritical CO_2 ($scCO_2$) process, whereby less-damaged GNs were obtained. They did not only find that the thickness and lateral size of the exfoliated GNs produced in the optimum SCFs conditions (45 °C, 150 bar) were 1.0–6.0 and 0.2–1.0 μm, but also the thinner GNs could be obtained by repeating the $scCO_2$ process. Hence, thickness control can be done by varying the number of $scCO_2$ in the process (Fig. 4).

Graphite conversion

Many research institutions are trying to develop ways to revolutionize the production of high-quality graphene sheet. One of the possible cost effective ways is through the reduction of GO to reduce graphene oxide (rGO). Rapid pyrolysis and surface modifications of graphite oxide or graphene oxide result in the formation of graphene nanosheets (Fig. 5).

Graphite oxide is a compound made up of carbon, hydrogen, and oxygen molecules. It is artificially created by treating graphite with strong oxidizers, such as sulphuric acid, H_2SO_4. These oxidisers function by reacting with the graphite and eliminating an electron in the chemical reaction. The most common methods used for creating graphite oxide are Hummers and Offeman [113] methods, in which, graphite is treated with a mixture of sulphuric acid (H_2SO_4), sodium nitrate ($NaNO_3$), and potassium permanganate ($KMnO_4$). Graphite oxide and graphene

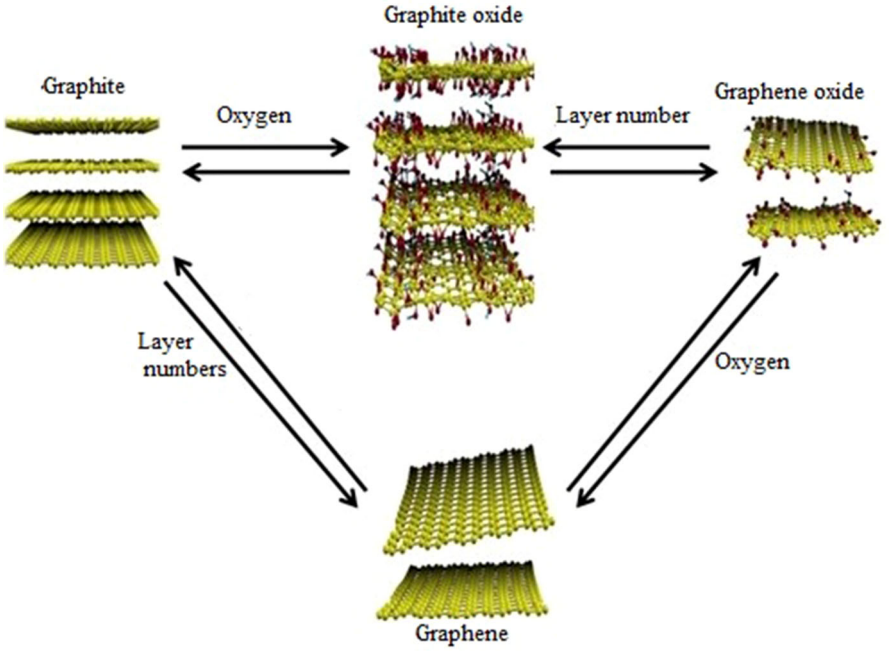

Fig. 5 The methods of graphene production

oxide are similar chemically, but different structurally. The main difference between graphite oxide and graphene oxide is the interplanar spacing between the individual atomic layers of the compounds caused by water intercalation. Graphite oxide is three dimensional, whereas graphene oxide is two dimensional. The oxidation process results in space formation, and also disrupts the sp^2 bonding network, which means that both graphite oxide and graphene oxide could be known as electrical insulators.

A few methods are possible to turn graphite oxide to graphene oxide. The most common techniques are using sonication, stirring, or a combination of the two. Sonication is a useful way in exfoliating graphite oxide and extremely successful at exfoliating graphene. Mechanical stirring is a less heavy approach, but it is time consuming to accomplish. Achaby et al. [114], in 2012, converted natural graphite to graphite oxide according to Hummer's method [113], followed by exfoliation of bulk graphite oxide to graphene oxide. The dried graphite oxide formed was dispersed in *N*,*N*-dimethylformamide (DMF) and ultrasonicated for 2 h [115, 116]. High-speed centrifugation of GO nanosheets suspension [116] was performed to isolate the solid phase.

Furthermore, there are several methods that can be used to reduce graphene oxide (GO) to produce reduced graphene oxide (rGO), which are treating GO with hydrazine [117–120], and sodium borohydrate ($NaBH_4$) [121, 122]. Hydrazine hydrate does not react with water and it is capable to produce very thin and fine graphite-like sheets [89]. Reduced graphene oxide becomes less hydrophilic due to

the removal of oxygen atom. $NaBH_4$ has been demonstrated to be more effective than hydrazine as a reductant of GO [122], although it can be slowly hydrolyzed by water and alcohol groups that remain after reduction. For a preferable method, Gao et al. [45], extended the dehydration process using 98 % of H_2SO_4 at 180 °C after reduction by $NaBH_4$ to further improve the reduction effect of GO.

Another safe method revealed by Fernández-Merino et al. [123], used ascorbic acid (vitamin C) as a substitute to hydrazine in the reduction of GO. In comparison with $NaBH_4$, vitamin C, pyrogallol, as well as heating under alkaline conditions, only vitamin C showed higher reduction than hydrazine. Besides being non-toxic, the suspensions of rGO synthesized using vitamin C can be prepared in water and in general solvent, such as DMF and *N*-methyl-2-pyrrolidone (NMP). Gao et al. [124], employed vitamin C as a reductant, and amino acid as a stabilizer to synthesize graphene and to give unique electrical properties similar to other methods.

The photo irradiation is another way of contributing to the reduction of GO. In 2013, Guo et al. [125], prepared rGO via green and scalable infrared (IR) irradiation induced photothermal reduction method. At high power density, the rGO becomes highly porous due to rapid degassing and exfoliation of GO sheets, thus revealing good performance as the anode material for lithium ion batteries. On the other hand, Williams et al. [126], found the UV irradiation also helps in reducing GO in TiO_2 suspensions and maintaining well-separated graphene-semiconductor composite sheets. The reduction is proved as the color of suspension shifted from brown to black. The interaction between TiO_2 particles and graphene sheets hinders the collapse of exfoliated graphene. The study was continued with the reduction of GO in ethanol interaction with excited ZnO nanoparticles [127]. In 2009, Cote et al. [128], used pulsed xenon flash from photographic camera that instantaneously triggered the deoxygenation reaction of GO at room temperature and it had been chemical free. The rapid microwave irradiation also can be employed to achieve exfoliation and reduction of graphite oxide within 1 min [129]. This method is scalable and cost effective (Fig. 6).

Besides, urea can be used as an expansion–reduction agent to synthesize graphene from graphite oxide [130]. This process consists of two simple steps: (1) graphite oxide is well mixed with urea that decomposes upon heating to release reducing gases, and (2) the mix is heated in an inert gas environment (e.g., N_2) for a

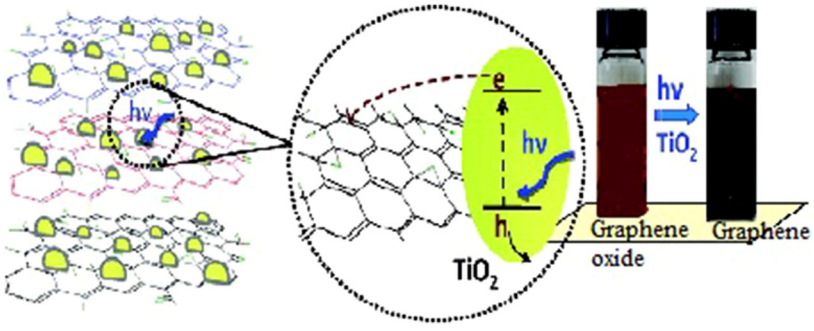

Fig. 6 TiO_2–graphene composite and its response under UV-excitation

short time in moderate temperature (ca. 600 °C). Then, upon cooling, the solid graphene is readily collected. Jin et al. [131], prepared nitrogen-doped graphene sheets (NGS) by annealing graphite oxide with urea under an Ar atmosphere for 3 h in a tubular furnace at 700–11,050 °C. The NGS is studied as positive electrode in vanadium redox flow battery.

Preparation methods of PLA/graphene-based nanocomposites

The preparation of polymer-based nanocomposites has become a great challenge in obtaining a good distribution of the nano-reinforcement. This level influences the quality of dispersion of filler in matrix; which in turn determines the properties of nanocomposites. The carbon nanotubes (CNT) have a tendency to form bundles that can be difficult to break down. This problem needs so much effort in developing methods of obtaining good distributions of CNT like chemical modifications [132]. Nonetheless, as for graphene or graphene oxide, the formation of bundles is not a problem although inclination of incomplete exfoliation and restacking can occur [133]. The mechanism for interaction in polymer/graphene nanocomposites relies on the polarity, molecular weight, hydrophobicity or reactive groups and other factors, which are present in the polymer, graphene or graphite, and solvent [134]. The incorporation of nanostructures into polymer can usually be done by three main strategies; in situ intercalative polymerization, solution intercalation, and melt intercalation.

In situ intercalative polymerization

In situ intercalative is a method where nanoparticles are first dispersed in liquid monomer or monomer solution, followed by the polymerization of monomers. The process assists in raising the interlayer spacing and exfoliates the layered structure of graphite into graphite nanoplates, and the intercalation of monomers generates polymer. In this method, a high level of dispersion of graphene-based filler is achieved without a prior exfoliation step, not likely in solution intercalation. Functionalized graphene or GO can improve the initial dispersion in the monomer liquid, and followed by in composite. This technique is applicable not only for the covalent bonding between functionalized sheets and polymer matrix through various condensation reactions, but also for non-covalent bonded composites, such as PP-GO [135], PE-graphite [136], and PMMA-GO [137]. The limitations of this method are the requirement of monomer units, as well as a lot of reagents for the polymerization procedure, and this results in less applicable for the case of naturally existing polymers.

Other than that, Yang et al. [138], prepared PLLA/thermally reduced graphene oxide composites via the in situ ring-opening polymerization of lactide, using thermally reduced graphene oxide as the initiator. Even though the in situ polymerization is an effective way to disperse the fillers in the matrix uniformly and to generate better interfacial interactions with the host polymer, the synthesis of high molecular weight in PLLA needs severe conditions [139, 140] and expensive

precursor (lactide) [140, 141]. In other works by Song et al. [142], and Yong et al. [143], PLLA was covalently grafted onto the convex surfaces and the tips of the multiwalled carbon nanotubes (MWNTs) via one step based on in situ polycondensation of L-lactic acid monomers. They prepared MWCNTs with carboxylic functional groups (MWCNTs–COOH) via a mixture of concentrated sulfuric acid and nitric acids oxidation. PLA is grafted on MWCNTs–COOH, which acted as an initiator.

Solution intercalation

This technique is based on solvent system, in which, the polymer or pre-polymer is solubilized and graphene or modified graphene layers are allowed to swell [144]. The common suitable solvents for graphene or modified graphene are water, acetone, chloroform, tetrahydrofuran, dimethyl formamide, and toluene, which bring the weak forces to stack the layers together. When the solvent is evaporated, the adsorbed polymer on the delaminated sheets will reassemble, sandwiching the polymer to form nanocomposites [145]. Basically, this process involves the mixing of colloidal suspensions of graphene-based material with the desired elastomer, either itself already in solution or by dissolving the elastomer in the same solvent used for filler dissolution, by simple stirring or shear mixing [146, 147]. Solution method is an effective fabrication technique due to the ease of processing graphite derivatives and graphene in water or organic solvents, but the solvent removal is a critical issue. Sonication is often practiced to aid in dispersion of graphitic fillers.

Cao et al. [147], dispersed the lyophilized graphene nanosheets (GNS) in DMF with the assistance of stirring and sonication at room temperature. They added 4 g of PLA and continued agitation at 85 °C in 2 h, and sonication at 70 °C for another 2 h. The study was carried out to compare the dispersion level between PLA/lyophilized GNS and PLA/vacuum-filtered GNS nanosheets. In 2011, DMF solution was used as solvent, followed by the sonication method, to prepare nanocomposites by Wang and Qiu [148] to identify the crystallization behaviors of poly(L-lactic acid)/GO nanocomposite, meanwhile Yoon et al. [149], studied different GO loading in poly(D,L-lactic-*co*-glycolic acid)/GO nanocomposite. On the other hand, Pinto et al. [150], prepared PLA/GO film nanocomposite using acetone solution, followed by ultrasonic bath for 5 h. Then, the solution was added to a PLA/chloroform solution and again sonicated for 15 min. They also prepared PLA/GNP films by dispersion in chloroform, then sonicated for 2 h, followed by redispersion in PLA/chloroform solution. The purpose of the research was to compare the biocompatibility, topography, roughness, and wettability between these two nanocomposites.

Melt intercalation

Graphene-based polymer nanocomposites can be composed via melt intercalation, in which, graphene is mixed when polymer is heated to molten state. The process avoids the use of toxic solvent and it is applicable using twin screw extruder, and two roll mills or internal mixer, which offers large-scale processing. Besides, both

polar and non-polar polymers are suitable for this method. However, since the pristine graphene has a tendency to agglomerate in polymer matrix, this method is unsuitable for intercalation by polymer chains. The stacking occurs due to the large ratio of surfaces of graphene sheets to their thickness, which brings to significant van der Waals forces and strong interaction between single sheets of graphene. The physical and chemical properties of such graphene aggregates are similar to the properties of graphite with relatively small surface area. The graphene functionalized through modification is preferred for melt intercalation. This has been supported by a few researches conducted, such as the preparation of PLA/EG [151–153]. Furthermore, Kim and Jeong [154] investigated the morphology, structure, thermal stability, mechanical, and electrical properties of PLA/exfoliated graphite through melt blending. On the other hand, Lei et al. [155], prepared conductive PLA with PMMA-functionalized graphene (PFG) by admicellar polymerization using melt-compounded machine at 180 °C for 10 min at a mixing speed of 80 rpm/min. The admicellar polymerization is a method of coating the graphene with nanofilms of polymers that is formed by polymerization of monomers inside the admicelles [156, 157]. This coating technique is purposed to redisperse graphene in water without any visible aggregation and to prevent the van der Waals from inducing the aggregation [158]. Wang et al. [159], prepared tricobalt tetraoxide-functionalized graphene nanofillers to reduce the fire hazards of PLA. Tricobalt tetraoxide (Co_3O_4) is proven in reducing the toxicity of pyrolysis gases in safety science and engineering applications by decreasing the CO concentration of the pyrolysis gases while burning [160]. The Co_3O_4/graphene nanofillers were produced by in situ chemical reduction process and were redispersed into PLA matrix by melt blending method.

PLA/graphene-based nanocomposites

Several researches have reported that graphene and graphene oxide (GO) have excellent electronic, thermal, and mechanical properties, and are expected to become essential materials in nanotechnology and various other engineering disciplines [161–165]. GO is expected to provide superiority, such as ease of dispersion in polymer matrixes, due to their oxygenated surface functionalities, causing stable dispersibility in aqueous or organic solutions by electrostatic repulsion [74, 115] and possible chemical interactions of oxygenated surface functionalities in GO nanosheets fabricated with polymer.

In addition, Kim and Jeong [154] investigated the morphology, structure, thermal stability, mechanical, and electrical properties of PLA/exfoliated graphite nanocomposites compared to PLA/micron-sized natural graphite (NG) composites. After melt-compounded with PLA matrix, SEM images and XRD patterns confirmed that the exfoliated graphite with 15 nm thickness were homogeneously dispersed in the PLA matrix, which is in contrast to the aggregates observed in the case of NG. The thermal degradation and Young's moduli of PLA/exfoliated graphite increased significantly with graphene content up to 3 wt%, however, the PLA/NG composites were unchanged regardless of the micron-sized graphite content. The electrical

percolation threshold of PLA/exfoliated graphite nanocomposites were shown to be far lower (was found be at 3–5 wt%) than PLA/NG (was found be at 10–15 wt% NG).

Besides, although the EG is not in nanoscale, the PLA/EG composites are discussed briefly since the expanded graphite is one of the graphene-based materials. Murariu et al. [151], produced PLA composites filled with EG. No significant effect was shown by EG loaded on polydispersity index compared to neat PLA, but the average molecular weight (M_n) indicated a decrease by increasing the EG loading from 2 to 6 wt%, which was caused by impurities, such as acidic species, metallic ions or residual products, that provoked PLA degradation during melt blending. Furthermore, graphite has excellent thermal stability and high thermal conductivity that can be as high as 3,000 Wm^{-1} K^{-1} [166], thus, influences the thermal and flame retardant mechanisms of the polymer matrix. As shown in Table 4, the PLA/EG nanocomposites indicate some extent of the temperatures for 5 or 50 wt% loss and maximum decomposition as compared to neat PLA. The layers of EG have the possibility to increase the diffusion pathway of the degradation of the by-products, and thus, creates good thermal stability to obstruct diffusion of volatile decomposition products. From the DSC analysis, the crystallinity of all PLA/EG nanocomposites is higher than neat PLA. The crystallinity increases with the addition of up to 6 % of EG, but for higher percentages in EG, the crystallinity decreases due to agglomeration and poor dispersion. From the dynamic mechanical analysis (DMTA), the PLA/EG nanocomposites lead to the enhancement of Young's modulus and storage modulus, thus, bring to the possibility to be used in applications that require higher temperature of utilization. The purification and pre-dispersion of EG nanofiller improve the mechanical performance of the nanocomposites. The nanocomposites also passed the horizontal test of UL94 HB with non-dripping and charring formation, besides decreasing the pHRR (30 wt% compared to neat PLA), which was proved via cone calorimetry testing.

Another research also used expanded graphite as filler. Hassouna et al. [152], prepared neat PLA and PLA/EG (3 wt%) nanocomposites at different rotor speed and time of melt blending. From the size-exclusion chromatography (SEC) analysis, the molecular masses of samples are as depicted in Table 5. The addition of EG affected the molecular weights of the PLA. Hassouna et al. concluded that there is

Table 4 TGA data of neat PLA compared to PLA/EG composites with different EG loading (under air flow, 20 °C/min (represents the value from [151])

Samples	Sample (%, by weight)	Temperature for 5 % weight loss, °C	Temperature for 50 % weight loss, °C	Temperature of the maximum rate of degradation, °C (from d-TGA)
1	PLA (granules)	339	373	377
2	PLA (processed)	335	372	378
3	PLA-4 % EG	340	377	382
4	PLA-8 % EG	345	380	385
5	PLA-12 % EG	347	383	385

Table 5 Molecular weights (M_n and M_w) of all the samples based on PLA (represents the value from [152])

Samples	M_n (g mol^{-1})	M_w (g mol^{-1})	Polydispersity index
PLA (granules)	77,000	204,300	2.65
PLA: 100 rpm, 10 min	65,400	202,300	3.92
PLA: 150 rpm, 10 min	61,600	194,500	3.15
PLA-3EG: 50 rpm, 5 min	93,000	227,200	2.44
PLA-3EG: 50 rpm, 10 min	96,500	228,400	2.36
PLA-3EG: 100 rpm, 10 min	119,000	243,000	2.04
PLA-3EG: 150 rpm, 10 min	121,700	249,200	2.05

M_n average molecular weight, M_w molecular weight

no general behavior in the expanded graphite towards a polymer matrix, in which it is introduced to. It mainly relies on the nature of the impurities present in EG and the processing conditions.

As for the study of morphology, the SEM images showed that better EG dispersion in PLA matrix was observed by increasing screw speed and residence time which led to better separation and shear. The TEM micrographs obtained also confirmed the observation made on SEM images. They used visible Raman spectroscopy as a tool for characterization because visible excitation resonates with the π states of carbon layers in graphene/graphite nanocomposites. The G band of Raman spectrum for pure EG was presented at 1,560 cm^{-1}, and the 2D band was around 2,700 cm^{-1}. The G and 2D bands of the PLA/3 wt% EG composites were upshifted with Raman shifted close to the graphite ones. The typical profile of 2D band was seen like 2D band in graphite samples [167], which suggested an increase in the interaction between the carbon layers. As the speed rate increased, the right side of the 2D was slightly upshifted, but the intensities of the G and 2D bands decreased, which were related to better dispersion of the fillers in the polymer. This filler dispersion was confirmed by SEM images. The residence time of blending EG in PLA; 5 and 10 min, did not influence the structure of the carbon fillers in PLA.

Moreover, Cao et al. [147], fabricated the lyophilized graphene nanosheets (GNS) by solution method with sonication. The comparisons in dispersion, morphology, and properties were made between vacuum-filtered GNS and lyophilized GNS. The vacuum-filtered GNS powders are paper-like materials, which failed to be dispersed in DMF might be due to the strong van der Waals forces between GNSs [147, 168]. The lyophilized GNS could be redispersed in organic solvents, such as DMF and *N*-methyl-2-pyrrolidone (NMP), which decreased the van der Waals forces, as proved by the XRD analysis and it can generate homogenous suspension. As for nanocomposites, the FESEM analysis confirmed that the GNSs are homogenously dispersed in PLA with no large-size aggregates observed and suggested intimate adhesion between GNSs and matrix. In thermal stability, the addition of 0.2 wt% GNSs increased more than 10 °C for 5 % weight loss. This improvement resulted by 'tortuous path' effect of GNS, which delayed the permeation of oxygen and the escape of volatile degradation products;

and also char permeation. Referring to mechanical properties, the 0.2 wt% GNS led to a 26 % increase in tensile strength and 18 % raise in Young's modulus due to efficient load transfer between PLA and GNS. The FESEM showed that the GNSs are embedded into host polymer with their flake-like morphology well remaining, which supported the strong adhesion between these two components.

On the other hand, Yoon et al. [149], studied the effect of GO loading on thermomechanical and surface chemical properties of poly(D,L-lactic-*co*-glycolic acid) (PLGA)/GO nanocomposites. They found that the average diameter of the nanocomposite nanofibers (contained 1 and 2 wt% of GO) was lower than the pristine PLGA. This attributed to large charge accumulations in solution jets caused by abundant negative charges on the surfaces, leading to strong electrostatic repulsion [169, 170]. The tensile moduli of PLGA/GO (1 wt%) and PLGA/GO (2 wt%) nanocomposite are significantly higher, almost 172.8 and 204.9 % than those of the pristine PLGA due to the strong interfacial interactions between nanofiller and polymer matrix caused by the dispersion of GO nanosheets and by chemical reactions of hydrogen bonding. They also revealed the ultimate tensile stresses, storage modulus (E'), and T_g of PLGA/GO (2 wt%) were higher than PLGA/GO (1 wt%). Besides, a biocompatibility test showed that the 2 wt% GO loading in nanocomposite enhanced the surface chemical properties, which effectively improved neuronal cell proliferation and viability. Furthermore, they found that the nanocomposite nanofibers were more hydrophilic than PLGA nanofibers due to the increased surface energy, which in turn led to improved biocompatibility [171, 172].

Furthermore, Wang and Qiu prepared a series of poly(L-lactic acid) (PLLA)/GO nanocomposites with different GO loading (0.5, 1 and 2 wt%) [144]. The non-isothermal melt crystallization peak temperatures from DSC analysis in nanocomposites were slightly higher than in pristine PLLA. The crystallization peak temperature (T_{cc}) of pristine PLLA was around 95.1 °C and shifted to about 97.0, 100.4, and 96.0 °C for 0.5, 1, and 2 wt% GO loading. This trend is also similar with isothermal melt crystallization temperatures, but it was maximum at 1 wt% GO loading. It was found that both non-isothermal and isothermal melt crystallization kinetics are enhanced in nanocomposites, which indicated that GO may act as a nucleating agent for crystallization of PLLA. Previously, similar findings were reported by Xu et al. [173]. They investigated the isothermal melt crystallization behaviors of PLLA induced by both graphene and CNT due to acceleration of PLLA by both nanoparticles. It was reported that the ability to accelerate crystallization by CNT is stronger by graphene. In another study, the cold crystallization behavior was analyzed at heating rates that ranged from 5 to 20 °C/min. The GO loading and heating rate are the factors that influenced the behavior. The non-isothermal cold crystallization peak temperature (T_p) of pristine PLLA was around 139.5 °C and shifted to around 130.9, 125.5, and 119.3 °C for the PLLA/GO nanocomposites with the increase of GO loading from 0.5 to 2 wt%, suggesting the T_p behavior of PLLA is enhanced significantly by the presence of GO in the PLLA/GO nanocomposites. In contrast, the T_p shifts to low temperature range with the decrease of heating rate for both neat PLLA and PLLA/GO nanocomposites. The glass transition (T_g) was around 61 °C for pristine PLLA and its nanocomposites

indicated that the GO does not affect T_g of PLLA apparently in the PLLA/GO nanocomposites. Besides, the isothermal cold crystallization kinetics, in a range of crystallization temperatures (T_cs) from 88 to 100 °C, was studied. It can be concluded that the crystallization time is reduced with the increase in crystallization temperature (T_c) for all pristine PLLA and PLLA/GO nanocomposites, which indicated that the crystallization rate becomes faster with the increase in T_c. For example, the crystallization time was reduced from around 16 min at 88 °C to 4.8 min at 100 °C for PLLA/GO (0.5 wt%). On the other hand, the crystallization time is declined with the increase in the GO loading for the PLLA/GO nanocomposites as compared to pristine PLLA, for example, at a T_c of 88 °C, it took around 19.1 min for pristine PLLA to complete crystallization, but it only took around 15.9, 11.2, and 9.0 min for 0.5, 1, and 2 wt% of GO loading, respectively. This suggests the presence of GO accelerates the isothermal cold crystallization of PLLA in the PLLA/GO nanocomposites. A similar trend can also be found at other T_cs. Instead, the crystallization mechanism and crystal structure remain unchanged for both pristine PLLA and PLLA/GO nanocomposites.

The effect of plasticizer on PLA blending was also studied by several researchers. The blending of origin PLA or mixing with other nanofillers produced brittle product. The plasticizer acts as a processing aid in flow improvement, mostly for films and cables. Instead of reducing the ductility, the plasticizer also functions in the mechanical and thermal properties enhancement. Plasticizers work by embedding themselves between the chains of polymers, spacing them apart, and thus, significantly lower the T_g for the plastic and makes it softer. A list of ester-like plasticizers for PLA has been studied, such as glucose monoesters, partial fatty acids, citrates, glycerol esters, and dicarboxylic esters [174–180]. Unfortunately, the low molecular weight plasticizers have the problem of migrating, owing to their high mobility within the PLA matrix. Therefore, the high molecular weight plasticizers with low mobility are suitable, such as poly(ethylene) glycol (PEG) [174, 181, 182], poly(propylene) glycol (PPG) [183], and atactic poly(3-hydroxybutyrate) (a-PHB) [184]. Besides lowering the T_g, they do not crystallize and miscible with PLA. Table 6 shows the recent studies using plasticizers, mostly PEG in PLA blends and their thermal analysis.

The choice of plasticizer used as a modifier for PLA is limited by legislative or the applications. On the other hand, the plasticizer has to be biodegradable, non-toxic for food contact (for packaging), and biocompatible (for medical applications). Commonly, the amount of plasticizers that range from 10 to 20 % is required to provide both a substantial reduction of T_g of the PLA matrix, and adequate mechanical properties. In environmental issues, the biodegradable or bioresorbable; and non-volatile plasticizer is preferred, with a relatively low molecular weight to produce the desired decrease of the Young's modulus value. Additionally, the ranging amount between 20 and 30 % of plasticizer in PLA matrix leads to phase separation. It must be remembered that the percentage of plasticizer determines the plasticization of PLA blend.

Table 6 Several studies of PLA blends, aided by plasticizers

Blend(s)	Material (M_n, average size/thickness/diameter)	Percentage of material loading	Method/Parameters of blending	Result for thermal analysis	Conclusion	References
PLA; PLA/PEGA	PLA = 200,000 g mol^{-1} PEGA = 550 g mol^{-1} DCP (as radical initiator)	PEGA = 10, 20, 30 and 40 wt% DCP = 0.8 wt%	Reactive blending using internal mixer (Haake)/180 °C in 5 min blending of PLA/PEGA, followed by 8 min blending after addition of DCP at 50 rpm	DSC analysis (comparisons were made between neat PLA and PLA/PEG up to 40 wt% loading): T_g is lowered from 59. 1 to 35.4 °C T_{cc} decreased from 113 to 81 °C T_m reduced from 169.6 to 163.1 °C X_c *(%)* increased with PEGA loading compared to neat PLA	The optimization of T_g and flexibility of blends could be done via controlling the grafted PEGA amount in PLA	[185]
PLA/rGO; PLA/xGnP; PLA/PEG/rGO; PLA/EPO/rGO; PLA/PEG/xGnP; PLA/EPO/xGnP	PLA = 183,000 g mol^{-1} PEG = 200 g mol^{-1} rGO = 15 μm (average size) xGnP = 6–8 nm (average thickness); =15 μm (average diameter)	xGnP = 0.3 wt% (fixed) rGO = 0.3 wt% (fixed)	Internal mixer (Brabender)/180 °C in 10 min at 50 rpm	TGA analysis: T_{50} and T_{max} of PLA/rGO were shifted up to about 10 and 6 °C compared to PLA/xGnP PLA/PEG/rGO blend showed improvement of 16 °C (T_{onset}), 15 °C (T_{50}), and 14 °C (T_{max}) compared to PLA/PEG/xGnP blend PLA/EPO/rGO blend showed improvement of 4 °C (T_{onset}), 3 °C (T_{50}), and 2 °C (T_{max}) compared to PLA/OPE/xGnP blend	Both PEG and EPO plasticizer enhanced the thermal degradation of PLA nanocomposites; rGO could act as good barrier to prevent thermal degradation of PLA compared to xGnP	[186]

Table 6 continued

Blend(s)	Material (M_n, average size/thickness/diameter)	Percentage of material loading	Method/Parameters of blending	Result for thermal analysis	Conclusion	References
PLA/PEG; PLA/PEG/xGnP	PLA = 183,000 g mol^{-1} PEG = 200 g mol^{-1} xGnP = 6–8 nm (average thickness); =15 μm (average diameter)	PLA/PEG = 90/10 wt% (fixed) xGnP = 0.1, 0.3, 0.5, 0.7 and 1.0 wt%	Internal mixer (Brabender)/160 °C in 10 min at 25 rpm	DSC analysis (comparisons were made between PLA/PEG and PLA/PEG/xGnP up to 1.0 wt% loading): T_g decreased from 51.63 to 50.45 °C T_{cc} increased from 74.30 to 78.26 °C (0.3 wt% xGnP), but decreased to 73.80 °C for further addition (1.0 wt%) T_m increased from 146.48 to 148.27 °C (0.5 wt% xGnP), but decreased to 147.30 °C for further addition (1.0 wt%) X_c (%) increased from 49.43 to 54.61 % TGA analysis (comparisons were made between PLA/PEG and PLA/PEG/0.5 wt% GnP): T_{onset} shifted from 194.5 to 250.4 °C: T_{max} shifted from 291.0 to 344.0 °C T_{50} shifted from 285.7 to 339.8 °C	xGnp enhanced the overall materials/s thermal stability and exhibit greater barrier effect to hinder the evaporation of the volatile degradation	[187]

PEGA poly(ethylene) glycol monoacrylate, *PEG* poly(ethylene) glycol), *DCP* dicumyl peroxide, *rGO* reduced graphene oxide, *xGnP* graphene nanoplatelets, *EPO* epoxidized palm oil, T_g glass transition temperature, T_{cc} cold crystallization temperature, T_m melting point temperature, X_c *(%)* crystallinity, T_{50} half decomposition temperature, T_{max} maximum decomposition, T_{onset} temperature onset

Conclusion

This review focused on the PLA/graphene-based nanocomposites specifically. The discussion covered three major topics: (1) route of producing graphene, (2) the processing methods, and (3) the properties of PLA/graphene-based nanocomposites. Graphene-based nanofiller are reinforcement materials that can improve mechanical, thermal, and electrical properties suitable for thermally and electrically conducting reinforced nanocomposites, electronic circuits, sensors, electrodes, etc. The discovery of graphene as nanofiller has opened a new dimension in the research field for the production of low cost, light weight, and high-reinforcement benefits, thus, bringing to a wide range of applications. The biomedical is the latest in the field of using graphene-based nanocomposites as biomedical devices. However, in obtaining good dispersions, the graphene–PLA interaction needs to be improved, which are achieved by the surface modification of graphene. There are a series of surface modification techniques that has been reported in this review. Hence, it can be concluded that the PLA/graphene-based nanocomposites exhibit superior mechanical properties compared to the neat PLA or conventional graphite-based composites. The improved properties of the nanocomposites were obtained at very low graphene contents ($\leq$2 wt%). The functional groups presented on graphene interrupt the π-conjugation in filler layers even at low loading and reduced the surface charge. This initiated the compatibility of PLA/filler that led to high electric properties for the composites. Thus, it is important to ensure that in the processing techniques to exfoliate graphene, such as sonication and thermal treatments, there are also possibilities for these methods to reduce electrical and thermal conductivities.

References

1. Novoselov KS, Geim AK, Morozov SV, Jiang D, Zhang Y, Dubonos SV et al (2004) Electric field effect in atomically thin carbon films. Science 306:666–669
2. Avéros L (2008) Polylactic acid: synthesis, properties and applications. In: Belgacem MN, Gandini A (eds) Book Chapter 21: Monomers, polymers, and composites from renewable resources. pp 433–50
3. Market Study Bioplastics, Ceresana, Dec 2011. www.ceresana.com/en/market-studies/plastics/bioplastics/
4. Doi Y, Steinbúchel A (2002) Biopolymers, applications and commercial products—polyesters III. Wiley-VCH, Weiheim, p 410
5. Södergárd A, Stolt M (2010) In Chapter 3: Industrial production of high molecular weight poly(lactic acid). In: Auras R, Lim LT, Selke SEM, Tsuji H (eds) Poly(lactic acid): synthesis, structures, properties, processing and applications. Wiley, New Jersey
6. Korhonen H, Helminen A, Seppala JV (2001) Synthesis of polylactide in the presence of co-initiators with different number of hydroxyl groups. Polymer 42:7541–7549
7. Han DK, Hubbell JA (1996) Lactide-based poly(ethylene glycol) polymer networks for scaffolds in tissue engineering. Macromolecules 29:5233–5235
8. Zhang X, MacDonald DA, Goosen MF, McAuley KB (1994) Mechanism of lactide polymerization in the presence of stannous octoate: The effect of hydroxyl and carboxylic acid substances. J Polym Sci Part A Polym Chem 32:2965–2970

9. Hyon SH, Jamshidi K, Ikada Y (1997) Synthesis of polylactide with different molecular weights. Biomaterials 18:1503–1508
10. Jacobsen S, Fritz HG, Degee P, Dubois P, Jerome R (2000) New developments on the ring-opening polymerization of polylactide. Ind Crops Prod 11(2–3):265–275
11. Rafier G, Lang J, Jobmann M, Bechthhold I (2003) Process for manufacturing homo and copolyesters of lactic acid. U.S. Patent 6,657,042, 2 Dec 2003
12. Griffith LG (2000) Polymeric biomaterials. Acta Mater 48:263–277
13. Cheng Y, Deng S, Chen P, Ruan R (2009) Polylactic acid (PLA) synthesis and modifications: a review. Front Chem China 4:259–264
14. Nampoothiri KM, Nair NR, John RP (2010) An overview of the recent developments in polylactide (PLA) research. Biores Technol 101:8493–8501
15. Södergárd A, Stolt M (2002) Properties of lactic acid based polymers and their correlation with composition. Prog Polym Sci (Oxford) 27:1123–1163
16. Auras R, Harte B, Selke S (2004) An overview of polylactides as packaging materials. Macromol Biosci 4:835–864
17. Oyama HT, Tanaka Y, Kadosaka A (2009) Rapid controlled hydrolytic degradation of poly(L-lactic acid) by blending with poly(aspartic acid-*co*-L-lactide). Polym Degrad Stab 94:1419–1426
18. Taubner V, Shishoo R (2001) Influence of processing parameters on the degradation of poly(L-lactide) during extrusion. J Appl Polym Sci 79:2128–2135
19. Anderson KS, Schreck KM, Hilmyer MA (2008) Toughening polylactide. Polym Rev 48:85–108
20. Mark JE (2009) Polymer data handbook. Oxford University Press, London, p 1264
21. Rasal RM, Janorkar AV, Hirt DE (2010) Poly(lactic) acid modifications. Prog Polym Sci 35:338–356
22. Clarinval AM, Halleux J (2005) Classification of biodegradable polymers. In: Smith R (ed) Biodegradable polymers for industrial applications, 1st edn. CRC Press, Boca Raton, FL, pp 3–31
23. Lim L-T, Auras R, Rubino M (2008) Processing technologies for poly(lactic acid). Prog Polym Sci 33:820–852
24. Fang Q, Hanna MA (1999) Rheological properties of amorphous and semicrystalline polylactic acid polymers. Ind Crops Prod 10:47–53
25. Dorgan JR, Lehermeier HJ, Mang M (2000) Thermal and rheological properties of commercial-grade poly(lactic acid)s. J Polym Environ 8:1–9
26. Lehermeier HJ, Dorgan JR (2000) Poly(lactic acid) properties and prospect of an environmentally benign plastic: melt rheology of linear and branched blends. In: Fourteenth symposium on thermophysical properties
27. Zhang W, Zheng S (2007) Synthesis and characterization of dendritic star poly(L-lactide)s. Polym Bull 58:767–775
28. Lehermeier HJ, Dorgan JR (2001) Melt rheology of poly(lactic acid): consequences of blending chain architectures. Polym Eng Sci 41:2172–2184
29. Heyrovska R (2008) Atomic structures of graphene, benzene and methane with bond lengths as sums of the single, double and resonance bond radii of carbon. Cornell University Library, USA
30. Brodie BC (1859) On the atomic weight of graphite. Philos Trans R Soc Lond 149:249–259
31. Hull AW (1917) A new method of X-ray crystal analysis. Phys Rev 10:661
32. Bernal JD (1924) The structure of graphite. Proc R Soc Lond A106:749–773
33. Boehm HP, Clauss A, Fischer G, Hofmann U (1962) In: Proceedings of the Fifth Conference on Carbon, Pergamon Press
34. DiVincenzo DP, Mele EJ (1984) Self-consistent effective mass theory for intralayer screening in graphite intercalation compounds. Phys Rev B 295:1685
35. Oshima C, Nagashima A (1997) Ultra-thin epitaxial films of graphite and hexagonal boron nitride on solid surfaces. J Phys Condens Matter 9:1
36. Novoselov KS et al (2005) Two-dimensional gas of massless dirac fermions in graphene. Nature 438:197–200
37. Gusynin VP, Sharapov SG (2005) Unconventional integer quantum Hall effect in graphene. Phys Rev Lett 9:146801
38. Zhang Y, Tan YW, Stormer HL, Kim P (2005) Experimental observation of the quantum Hall effect and Berry's phase in graphene. Nature 438:201–204
39. Meyer J et al (2007) The structure of suspended graphene sheets. Nature 446:60–63
40. Geim AK, Kim P (2008) Carbon wonderland. Sci Amer 298:90–97

41. The Nobel Prize in Physics 2010. *Nobelprize.org*. Nobel Media AB 2014. http://www.nobelprize.org/nobel_prizes/physics/laureates/2010. Retrieved 25 Jan 2015
42. Li J-L, Kudin KN, McAllister MJ, Prud'homme RK, Aksay IA, Car R (2006) Oxygen-driven unzipping of graphitic materials. Phys Rev Lett 96:176101
43. Suk JW, Piner RD, An J, Ruoff RS (2010) Mechanical properties of monolayer graphene oxide. ACS Nano 4:6557–6564
44. Mahanta NK, Abramson AR (2012) Thermal conductivity of graphene and graphene oxide nanoplatelets. Thermal and Thermomechanical Phenomena in Electronic Systems (ITherm) 2012 13th IEEE Intersociety Conference on 2012, pp 1–6
45. Gao W, Alemany LB, Ci L, Ajayan PM (2009) New insights into the structure and reduction of graphite oxide. Nat Chem 1:403–408
46. Kuila T, Bose S, Mishra AK, Khanra P, Kim NH, Lee JH (2012) Chemical functionalization of graphene and its applications. Prog Mater Sci 57:1061–1105
47. Afanasov IM, Morozov VA, Kepman AV, Ionov SG, Seleznev AN, Tendeloo GV, Avdeev VV (2009) Preparation, electrical and thermal properties of new exfoliated graphite-based composites. Carbon 47:263–270
48. Nair RR, Blake P, Grigorenko AN, Novoselov KS, Booth TJ, Stauber T, Peres NMR, Geim AK (2008) Fine structure constant defines visual transparency of graphene. Sci 320:1308
49. Ma X, Tao H, Yang K, Feng L, Cheng L, Shi X, Li Y, Guo L, Liu Z (2012) A functionalized graphene oxide-iron oxide nanocomposite for magnetically targeted drug delivery, photothermal therapy and magnetic resonance imaging. Nano Res 5:199–212
50. Shen A-J, Li D-L, Cai X-J, Dong C-Y, Dong H-Q, Wen H-Y, Dai G-H, Wang P-J, Li Y-Y (2012) Multifunctional nanocomposite based on graphene oxide for in vitro hepatocarcinoma diagnosis and treatment. J Biomed Mater Res A 100A:2499–2506
51. Goenka S, Sant V, Sant S (2014) Graphene-based nanomaterials for drug delivery and tissue engineering. J Controll Release 173:75–88
52. Hsieh C-T, Chen WY (2011) Water/oil repellency and work of adhesion of liquid droplets on graphene oxide and graphene surfaces. Surf Coat Technol 205:4554–4561
53. Hasan SA, Rigueur JL, Harl RR, Krejci AJ, Gonzalo-Juan I, Rogers BR, Dickerson JH (2010) Transferable graphene oxide films with tunable microstructures. ACS Nano 4:7367–7372
54. Yang S-T, Chang Y, Wang H, Liu G, Chen S, Wang Y, Liu Y, Cao A (2010) Folding/aggregation of graphene oxide and its application in Cu^{2+} removal. J Colloid Interface Sci 351:122–127
55. Cote LJ, Kim F, Huang J (2008) Langmuir–Blodgett assembly of graphite oxide single layers. J Am Chem Soc 131:1043–1049
56. Segal M (2009) Selling graphene by the ton. Nat Nanotech 4:612–614
57. EUROPA-PRESS RELEASES. Graphene and Human Brain Project win largest research excellence award in history, as battle for sustained science funding continues. Europa.eu 28-01-2013
58. Xuan Y, Wu YQ, Shen T et al (2006) Atomic-layer graphene gilms. Phys Rev Lett 97:036803–036806
59. Liang X (2014) Ch. 19: Transition from tubes to sheets—a comparison of the properties and applications of carbon nanotubes and graphene. Nanotube superfiber materials: changing engineering design. pp 519–68
60. Yang XM, Tu YF, Li L et al (2010) Well-dispersed chitosan/graphene oxide nanocomposites. ACS Appl Mater Interfaces 2:1707–1713
61. Fan HL, Wang LL, Zhao KK et al (2010) Fabrication, mechanical properties, and biocompatibility of graphene-reinforced chitosan composites. Biomacromolecules 11:2345–2351
62. Bai H, Li C, Wang XL et al (2010) A pH-sensitive graphene oxide composite hydrogel. Chem Commun 46:2376–2378
63. Sun ST, Wu PY (2011) A one-step strategy for thermal- and pH-responsive graphene oxide interpenetrating polymer hydrogel networks. J Mater Chem 21:4095–4097
64. Liu C, Alwarappan S, Chen ZF et al (2010) Membraneless enzymatic biofuel cells based on graphene nanosheets. Biosens Bioelectron 25:1829–1833
65. Stoller MD, Park S, Zhu YW et al (2008) Graphene-based ultracapacitors. Nano Lett 8:3498–3502
66. Wang L, Lee K, Sun YY et al (2009) Graphene oxide as an ideal substrate for hydrogen storage. ACS Nano 121:4879–4881
67. Goli P, Legedza S, Dhar A, Salgado R, Renteria J, Balandin AA (2014) Graphene-enhanced hybrid phase change materials for thermal management of Li-ion batteries. J Power Sources 248:37–43

68. Lu CH, Yang HH, Zhu CL et al (2009) A graphene platform for sensing biomolecules. Angew Chem Int Ed 121:4879–4881
69. Zhu L, Jia Y, Gai G, Ji X, Luo J, Yao Y (2014) Ambipolarity of large-area Pt-functionalized graphene observed in H2 sensing. Sens Actuators B Chem 190:134–140
70. Qu LT, Liu Y, Baek JB et al (2010) Nitrogen-doped graphene as efficient metal-free electrocatalyst for oxygen reduction in fuel cells. ACS Nano 4:1321–1326
71. Wang H, Yuan X, Wu Y, Huang H, Peng X et al (2013) Graphene-based materials: fabrication, characterization and application for the decontamination of wastewater and waste gas and hydrogen storage/generation. Adv Colloid Interface Sci 195–196:19–40
72. Ji Z, Shen X, Yang J, Zhu G, Chen K (2014) A novel reduced graphene oxide/Ag/CeO_2 ternary nanocomposite: green synthesis and catalytic properties. Appl Catal B 144:454–461
73. Liu Z, Robinson JT, Sun X, Dai H (2008) PEGylated nanographene oxide for delivery of water-insoluble cancer drugs. J Am Chem Soc 130:10876–10877
74. Sun XM, Liu Z, Welsher K et al (2008) Nano-graphene oxide for cellular imaging and drug delivery. Nano Res 1:203–212
75. Loh KP, Bao QL, Eda G et al (2010) Graphene oxide as a chemically tunable platform for optical applications. Nat Chem 2:1015–1024
76. Jing W, Yin-song W, Xiao-ying Y, Yuan-yuan I, Jin-rong Y, Rui Y, Ning Z (2012) Graphene oxide used a carrier for adriamycin can reverse drug resistance in breast cancer cells. Nanotech 23:355101
77. Yang ZR, Wang HF, Zhao J et al (2007) Recent developments in the use of adenoviruses and immunotoxins in cancer gene therapy. Cancer Gene Ther 14:599–615
78. Shen H, Zhang L, Liu M, Zhang Z (2012) Biomedical applications of graphene. Theranostics 2:283–294
79. Zhang L, Lu Z, Zhao Q, Huang J, Shen H, Zhang Z (2011) Enhanced chemotherapy efficacy by sequential delivery of siRNA and anticancer drugs using PEI-grafted graphene oxide. Small 7:460–464
80. Chen B, Liu M, Zhang L, Huang J, Yao J, Zhang Z (2011) Polyethylenimine-functionalized graphene oxide as an efficient gene delivery vector. J Mater Chem 21:7736–7741
81. Feng L, Zhang S, Liu Z (2011) Graphene based gene transfection. Nanoscale 3:1252–1257
82. Kim H, Namgung R, Singha K, Oh I-K, Kim WJ (2011) Graphene oxide-polyethylenimine nano-construct as a gene delivery vector and bioimaging tool. Bioconjug Chem 22:2558–2567
83. Bao HQ, Pan YZ, Ping Y et al (2011) Chitosan-functionalized graphene oxide as a nanocarrier for drug and gene delivery. Small 7:1569–1578
84. Shen H, Liu M, He H, Zhang L, Huang J, Chong Y, Dai J, Zhang Z (2012) PEGylated graphene oxide-mediated protein delivery for cell function regulation. ACS Appl Mat Interfaces 4:6317–6323
85. Somani PR, Somani SP, Umeno M (2006) Planer nano-graphenes from camphor by CVD. Chem Phys Lett 430:56–59
86. Kim KS, Zhao Y, Jang H, Lee YS, Kim JM et al (2009) Large-scale pattern growth of graphene films for stretchable transparent electrodes. Nat 457:706–710
87. Li X, Cai W, An J, Kim S, Nah J, Yang D et al (2009) Large-area synthesis of high-quality and uniform graphene films on copper foils. Sci 324:1312–1314
88. Reina A, Jia X, Ho J, Nezich D, Son H, Bulovic V et al (2008) Large area, few-layer graphene films on arbitrary substrates by chemical vapor deposition. Nano Lett 9:30–35
89. Singh V, Joung D, Zhai L, Das S, Khondaker SI, Seal S (2011) Graphene based materials: past, present and future. Prog Mater Sci 56:1178–1271
90. Wei D, Liu Y, Wang Y, Zhang H, Huang L, Yu G (2009) Synthesis of N-doped graphene by chemical vapour deposition and its electrical properties. Nano Lett 9:1752–1758
91. Reddy ALM, Srivasta A, Gowda SR, Gullapalli H, Dubey M, Ajayan PM (2010) Synthesis of nitrogen-doped graphene films for lithium battery applications. ACS Nano 4:6337–6342
92. Terasawa T, Saiki K (2012) Growth of graphene on Cu by plasma enhanced chemical vapour deposition. Carbon 50:869–874
93. Sutter P (2009) Epitaxial graphene: how silicon leaves the scene. Nat Mater 8:171–172
94. Patterned thin film graphite devices and method for making same. US Patern 7015142
95. Moon JS et al (2009) Epitaxial-graphene RF field-effect transistors on Si-face 6H-SiC substrates. IEEE Electro Device Lett 30:650–652
96. Kedzierski J et al (2008) Epitaxial graphene transistors on Sic substrates. IEEE Trans Electron Devices 55:2078–2085

97. Parga ALVD, Calleja F, Borca BMCG, Passeggi J, Hinarejos JJ, Guinea F et al (2008) Periodically rippled graphene: growth and spatially resolved electronic structure. Phys Rev Lett 100:056807
98. Pletikosić I, Kralj M, Brako R, Coraux J, N'Diaye AT, Busse C, Michely T (2009) Dirac cones and minigaps for graphene on Ir (1 1 1). Phys Rev Lett 102:056808
99. Rafiee J, Mi X, Gullapalli H, Thomas AV, Yayari F, Shi Y, Ajayan PM, Koratkar NA (2012) Wetting transparency of graphene. Nat Mater 11:217–222
100. Wassei JK, Mecklenburg M, Torres JA, Jesse DF, Regan BC, Richard BK, Bruce HW (2012) Chemical vapour deposition of graphene on copper from methane, ethane and propane: evidence for bilayer selectivity. Small 8:1415–1422
101. Sun Z, Yan Z, Yao J, Beitler E, Zhu Y, Tour JM (2010) Growth of graphene from solid carbon sources. Nat 468:549–552
102. Sadasivuni KK, Ponnamma D, Thomas S, Grohens Y (2013) Evolution from graphite to graphene elastomer composites. Prog Polym Sci. doi:10.1016/j.progpolymsci.2013.08.003
103. Hassan M, Reddy KR, Haque E, Minett AI, Gomes VG (2013) High-yield aqueous phase exfoliation of graphene for facile nanocomposite synthesis via emulsion polymerization. J Colloid Interf Sci 410:43–51
104. Zhou K, Shi Y, Jiang S, Song L, Hu Y, Ghui Z (2013) A facile liquid exfoliation method to prepare graphene sheets with different sizes expandable graphite. Mater Res Bull 48:2985–2992
105. Terrones M, Botello-Méndez AR, Campos-Delgado J, López-Urías F, Vega-Cantú YI et al (2010) Graphene and graphite nanoribbons: morphology, properties, synthesis, defects and applications. Nanotoday 5:351–372
106. Chakrabarti A, Lu J, Sakrabutenas JC, Xu T, Xiao Z, Maquire JA, Hosmane NS (2011) Conversion of carbon dioxide to few-layer graphene. J Mater Chem 21:9491–9493
107. Zhao WF, Fang M, Wu H, Wang LW, Chen GH (2010) Preparation of graphene by exfoliation of graphite using wet ball milling. J Mater Chem 20:5817–5819
108. Leon V, Quintana M, Herrero MA, Fierro JLG, de la Hoz A, Prato M et al (2011) Few-layer graphenes from ball-milling of graphite with melamine. Chem Commun 47:10936–10938
109. Zhao WF, Wu FE, Wu H, Chen GH (2010) Preparation of colloidal dispersions of graphene sheets in organic solvents by using ball milling. J Nanometer. doi:10.1155/2010/528235
110. Pu NW, Wang CA, Sung Y, Liu YM, Ger MD (2009) Production of few-layer graphene by supercritical CO(2) exfoliation of graphite. Mater Lett 63:1987–1989
111. Rangappa D, Sone K, Wang MS, Gautam UK, Goldberg D, Itoh H et al (2010) Rapid and direct conversion of graphite crystals into high-yielding, good-quality graphene by supercritical fluid exfoliation. Chem Eur J 16:6488–6494
112. Sim HS, Kim TA, Lee KH, Park M (2012) Preparation of graphene nanosheets through repeated supercritical carbon dioxide process. Mater Lett 89:343–346
113. Hummers WS Jr, Offeman RE (1957) Preparation of graphitic oxide. J Am Chem Soc 80:1339
114. Achaby ME, Arrakhiz FZ, Vaudreuil S, Essassi EM, Qaiss A (2012) Piezoelectric β-polymorph formation and properties enhancement in graphene oxide-PVDF nanocomposite films. Appl Surf Sci 258:7668–7677
115. Parades JI, Villar-Rodil S, Martinez-Alonso A, Tascon JMD (2008) Graphene oxide dispersion in organic solvent. Langmuir 24:10560–10564
116. Chen D, Zhu H, Liu T (2010) In situ thermal preparation of polyimide nanocomposite films containing functionalized graphene sheets. ACS Appl Mater Interfaces 2:3702–3708
117. Pei S, Cheng H-M (2012) The reduction of graphene oxide. Carbon 50:3210–3228
118. Eda G, Fanchini G, Chhowalla M (2008) Large-area ultrathin films of reduced graphene oxide as a transparent and flexible electronic material. Nature Nanotechnol 3:270–274
119. Gomez-Navarro C, Weitz RT, Bittner AM, Scolari M, Mews A, Burghard M et al (2007) Electronic transport properties of individual chemically reduced graphene oxide sheets. Nano Lett 7:3449–3503
120. Lee C-G, Park S, Ruoff RS, Dodabalapor A (2009) Integration of reduced graphene oxide into organic field-effect transistors as conducting electrodes and as a metal modification layer. Appl Phys Lett 95:023304
121. Bourlinos AB, Gournis D, Petridis D, Szabó T, Szeri A, Dékány I (2003) Graphite oxide: chemical reduction to graphite and surface modification with aliphatic amines and amino acids. Langmuir 19:6050–6055

122. Shin H-J, Kim KK, Benayad A, Yoon S-M, Park HK, Jung I-S et al (2009) Efficient reduction of graphite oxide by sodium borohydride and its effect on electrical conductance. Adv Funct Mater 19:1987–1992
123. Fernández-Merino MJ, Guardia L, Paredes JI, Villar-Rodil S, Solís-Fernández P, Martínez-Alonso A, Tascón JMD (2010) Vitamin C is an ideal substitute for hydrazine in the reduction of graphene oxide suspensions. J Phys Chem 114:6426–6432
124. Gao J, Liu F, Liu Y, Ma N, Wang Z, Zhang X (2010) Environment-friendly method to produce graphene that employs vitamin C and amino acid. Chem Mater 22:2213–2218
125. Guo H, Peng M, Zhu Z, Sun L (2013) Preparation of reduced graphene oxide by infrared irradiation induced photothermal reduction. Nanoscale 5:9040–9048
126. Williams G, Seger B, Kamat PV (2008) TiO_2-graphene nanocomposites. UV-assisted photocatalytic reduction of graphene oxide. ACS Nano 2:1487–1491
127. Williams G, Kamat PV (2009) Graphene-semiconductor nanocomposites: excited-state interactions between ZnO nanoparticles and graphene oxide. Langmuir 25:13869–13873
128. Cote LJ, Cruz-Silva R, Huang J (2009) Fush reduction and patterning of graphite oxide and its polymer composite. J Am Chem Soc 131:11027–11032
129. Zhu Y, Murali S, Stoller MD, Velamakanni A, Piner RD, Ruoff RS (2010) Microwave assisted exfoliation and reduction of graphite oxide for ultracapacitors. Carbon 48:2118–2122
130. Wakeland S, Martinez R, Grey JK, Luhrs CC (2010) Production of graphene from graphite oxide using urea as expansion-reducing agent. Carbon 48:3463–3470
131. Jin J, Fu X, Liu Q, Liu Y, Wei Z, Niu K, Zhang J (2013) Identifying the active site in nitrogen-doped graphene for the VO^{2+}/VO_2^{+} redox reaction. ACS Nano 7:4764–4773
132. Roy N, Sengupta R, Bhowmick A (2012) Modifications of carbon for polymer composites and nanocomposites. Prog Polym Sci 37:781–819
133. Young RJ, Kinloch IA, Gong L, Novoselov KS (2012) The mechanics of graphene nanocomposites: a review. Compos Sci Tecnol 72:1459–1476
134. Zhang HB, Zheng WG, Yan Q, Yang Y, Wang J, Lu ZH et al (2010) Electrically, conductive polyethylene terephthalate/graphene nanocomposites prepared by melt blending. Polymer 51:1191–1196
135. Huang Y, Qin Y, Zhou Y, Niu H, Yu Z-Z, Dong J-Y (2010) Poly propylene/graphene oxide nanocomposites prepared by in situ Ziegler–Natta polymerization. Chem Matter 22:4096–4102
136. Fim FDC, Guterres JM, Basso NRS, Galland GB (2010) Polyethylene/graphite nanocomposites obtained by in situ polymerization. J Polym Sci Part A Polym Chem 48:692–698
137. Jang JY, Kim MS, Jeong HM, Shin CM (2009) Graphite oxide/poly(methyl methacrylate) nanocomposites prepared by a novel method utilizing macroazoinitiator. Compos Sci Technol 69:186–191
138. Yang J-H, Lin S-H, Lee Y-D (2012) Preparation and characterization of poly(L-lactide)-graphene composites using the in situ ring-opening polymerization of PLLA with graphene as the initiator. J Mater Chem 22:10805
139. Garlotta D (2001) A literature review of poly(lactic acid). J Polym Environ 9:63–84
140. Li W, Xu Z, Chen L, Shan M, Tian X et al (2014) A facile method to produce graphene oxide-g-poly(L-lactic acid) as an promising reinforcement for PLLA nanocomposites. Chem Eng J 237:291–299
141. Achmad F, Yamane K, Quan S, Kokugan T (2009) Synthesis of polylactic acid by direct polycondensation under vacuum without catalysts, solvents and initiators. Chem Eng J 151:342–350
142. Song W, Zheng Z, Tang W, Wang X (2007) A facile approach to covalently functionalized carbon nanotubes with biocompatible polymer. Polymer 48:3658–3663
143. Yoon JT, Jeong YG, Lee SC, Min BG (2009) Influences of poly(lactic acid)-grafted carbon nanotube on thermal, mechanical and electrical properties of poly(lactic acid). Polym Adv Technol 20:631–638
144. Stankovich S, Dikin DA, Dommett GHB, Kohlhaas KM, Zimney EJ, Stach EA et al (2006) Graphene-based composite materials. Nature 442:282–286
145. Lee WD, Im SS (2007) Thermomechanical properties and crystallization behavior of layered double hydroxide hydroxide/poly(ethylene terephthalate) nanocomposites prepared by in situ polymerization. J Polym Sci Part B Polym Phys 45:28–40
146. Sing VK, Shukla A, Patra MK, Saini L, Jani RK, Vadera SR, Kumar N (2012) Microwave absorbing properties of a thermally reduced graphene oxide/nitrile butadiene rubber composite. Carbon 50:2022–2028

147. Cao Y, Feng J, Wu P (2010) Preparation of organically dispersible graphene nanosheet powders through a lyophilization method and their poly(lactic acid) composites. Carbon 48:3834–3839
148. Wang H, Qiu Z (2011) Crystallization behaviours biodegradable poly(L-lactic acid)/graphene oxide nanocomposites from the amorphous state. Thermochim Acta 526:229–236
149. Yoon OJ, Jung CY, Sohn IY, Kim HJ, Hong B et al (2011) Nanocomposite nanofibers of poly(D, L-lactic-co-glycolic acid) and graphene oxide nanosheets. Compos Part A 42:1978–1984
150. Pinto AM, Moreira S, Gonçalves IC, Gama FM, Mendes AM, Magalhães FD (2013) Biocompatibility of poly(lactic acid) with incorporated graphene-based materials. Colloids Surf B Biointerfaces 104:229–238
151. Murariu M, Dechief AL, Bonnaud L, Paint Y, Gallos A, Fontaine G et al (2010) The production and properties of polylactide composites filled with expanded graphite. Polym Degrad Stab 95:889–900
152. Hassouna F, Laachachi A, Chapron D, Moedden YE, Toniazzo V, Ruch D (2011) Development of new approach based on Raman spectroscopy to study the dispersion of expanded graphite in poly(lactide). Polym Degrad Stab 96:2040–2047
153. Antar Z, Feller JF, Noël H, Glouannec P, Elleuch K (2012) Thermoelectric behaviour of melt processed carbon nanotube/graphite/poly(lactic acid) conductive biopolymer nanocomposites (CPC). Mater Lett 67:210–214
154. Kim IH, Jeong YG (2010) Polylactide/exfoliated graphite nanocomposites with enhanced thermal stability, mechanical modulus, and electrical conductivity. J Polym Sci Part B Polym Phys 48:850–858
155. Lei L, Qiu J, Sakai E (2012) Preparing conductive poly(lactic acid)(PLA) with poly(methyl methacrylate)(PMMA) functionalized graphene (PFG) by admicellar polymerization. Chem Eng J 209:20–27
156. Yooprasert N, Pongprayoon T, Suwanmala P, Hemvichian K, Tumcharem G (2010) Radiation-induced admicellar polymerization of isoprene on silica: effects of surfactant's chain length. Chem Eng J 156:193–199
157. Maity J, Kothary P, O'Rear EA, Jacob C (2010) Preparation and comparison of hydrophobic cotton fabric obtained by direct fluorination and admicellar polymerization of fluoromonomers. Ind Eng Chem Res 49:6075–6079
158. Das S, Wajid AS, Shelburne JL, Liao YC, Green MJ (2011) Localized in situ polymerization on graphene surfaces for stabilized graphene dispersions. ACS Appl Mater Interfaces 3:1844–1851
159. Wang X, Song L, Yang YH, Xing WY, Lu HD, Hu Y (2012) Cobalt oxide/graphene composite for highly efficient CO oxidation and its application in reducing the fire hazards of aliphatic polyesters. J Mater Chem 22:3426–3431
160. Xie X, Li Y, Liu ZQ, Haruta M, Shen W (2009) Low-temperature oxidation of CO catalysed by Co_3O_4 nanorods. Nature 458:746–749
161. Zhu Y, Murali S, Cai W, Li X, Suk JW, Potts JR et al (2010) Graphene and graphene oxide: synthesis, properties and applications. Adv Mater 22:3906–3924
162. Compton OC, Nguyen ST (2010) Graphene oxide, highly reduced graphene oxide, and graphene: versatile building blocks for carbon-based materials. Small 6:711–723
163. Huang KJ, Niu DJ, Sun JY, Han CH, Wu ZW, Li YL et al (2010) Novel electrochemical sensor based on functionalized graphene for simultaneous determination of adenine and guanine in DNA. Colloids Surf B Biointerfaces 82:543–549
164. Ang PK, Jaiswal M, Lim CH, Wang Y, Sankaran J, Li A et al (2010) A bioelectronic platform using a graphene–lipid bilayer interface. ACS Nano 4:7387–7394
165. Ryoo SR, Kim YK, Kim MH, Min DH (2010) Behaviors of NIH-3T3 Fibroblasts on graphene/carbon nanotubes: proliferation, focal adhesion and gene transfection studies. ACS Nano 4:6587–6598
166. Fukushima H, Drzal LT, Rook BP, Rich MJ (2006) Thermal conductivity of exfoliated graphite nanocomposites. J Therm Anal Calorim 85:235–238
167. Cancadoa LG, Takaia K, Enokia T, Endob M, Kimb Y, Mizusakib H et al (2008) Measuring the degree of stacking order in graphite by Raman spectroscopy. Carbon 46:272–275
168. Stankovich S, Dikin DA, Piner RD, Kohlhaas KA, Kleinhammes A, Jia Y et al (2007) Synthesis of graphene-based nanosheets via chemical reduction of exfoliated graphite oxide. Carbon 45:1558–1565
169. Singh R, Pantarotto D, Lacerda L, Pastorin G, Klumpp C, Prato M et al (2006) Tissue biodistribution and blood clearance rates of intravenously administered carbon nanotube radiotracers. PNAS 103:3357–3362

170. Si Y, Samulski ET (2008) Synthesis of water soluble graphene. Nano Lett 8:1679–1682
171. Yoon OJ, Kim HW, Kim DJ, Lee HJ, Yun JY, Noh YH et al (2009) Nanocomposites of electrospun poly(D, L-lactic)-*co*-(glycolic acid) and plasma-functionalized single-walled carbon nanotubes for biomedical applications. Plasma Process Polym 6:101–109
172. Chen C, Liang B, Lu D, Ogino A, Wang X, Nagatsu M (2010) Amino group introduction onto multiwall carbon nanotubes by NH_3/Ar plasma treatment. Carbon 48:939–948
173. Xu J, Chen T, Yang C, Li Z, Mao Y et al (2010) Isothermal crystallization of poly(L-lactide) induced by graphene nanosheets and carbon nanotubes: a comparative study. Macromolecules 43:5000–5008
174. Jacobsen S, Fritz HG (1999) Plasticizing polylactide—the effect of different plasticizers on the mechanical properties. Polym Eng Sci 39:1303–1310
175. Martin O, Averous L (2001) Poly(lactic acid): plasticization and properties of biodegradable multiphase systems. Polymer 42:6209–6219
176. Oksman K, Skrifvars M, Selin JF (2003) Natural fibres as reinforcement in polylactic acid (PLA) composites. Comp Sci Tech 63:1317–1324
177. Ljungberg N, Andersson T, Wesslen B (2003) Film extrusion and film weldability of poly(lactic acid) plasticized with triacetin and tributyl citrate. J Appl Polym Sci 88:3239–3247
178. Ljungberg N, Wesslen B (2005) Preparation and properties of plasticized poly(lactic acid) films. Biomacromolecules 6:1789–1796
179. Ljungberg N, Wesslen B (2003) Tributyl citrate oligomers as plasticizers for poly(lactic acid): thermo-mechanical film properties and aging. Polymer 44:7679–7688
180. Murariu M, Ferreira ADS, Pluta M et al (2008) Polylactide (PLA)–CaSO4 composites toughened with low molecular weight and polymeric-ester like plasticizers and related performances. Euro Polym J 44:3842–3852
181. Hu Y, Hu YS, Topolkaraev V, Hiltner A, Baer E (2003) Crystallization and phase separation in blends of high stereoregular poly(lactide) with poly(ethene glycol). Polymer 44:5681–5689
182. Hu Y, Rogunova M, Topolkaraev V, Hiltner A, Baer E (2003) Ageing of poly(lactide)/poly(ethylene glycol) blends. Part 1. Poly(lactide) with low stereoregularity. Polymer 44:5701–5710
183. Kulinski Z, Piorkowska E, Gadzinowska K, Stasiak M (2006) Plasticization of poly(lactide) with poly(propylene glycol). Biomacromolecules 7:2128–2135
184. Focarete ML, Scandola M, Dobrzynski MS, Kowalczuk M (2002) Miscibility and mechanical properties of blends of (L)-lactide copolymers with atactic poly(3-hydroxybutyrate). Macromolecules 35:8472–8477
185. Choi K-M, Choi M-C, Han D-H et al (2013) Plasticization of poly(lactic acid) (PLA) through chemical grafting of poly(ethylene glycol) (PEG) via in situ reactive blending. Euro Polym J 49:2356–2364
186. Chieng BW, Ibrahim N, Yunus WMZW et al (2014) Effects of graphene nanoplatelets and reduced graphene oxide on poly(lactic acid) and plasticized poly(lactic acid): a comparison study. Polymers 6:2232–2246
187. Chieng BW, Ibrahim N, Yunus WMZW, Hussein MZ (2014) Poly(lactic acid)/poly(ethylene glycol) polymer nanocomposites: effects of graphene nanoplatelets. Polymers 6:93–104